Through a Glass Clearly: The Challenge of Glass 3D-printing

Michael P. Avery,^{1,2} Susanne Klein,^{3} Robert Richardson,^{2} Paul Bartlett,^{2} Steve Simske^{4}
^{1}Bristol Centre for Functional Nanomaterials (UK), ^{2}University of Bristol (UK), ^{3}HP labs Bristol (UK), ^{4}HP Labs Fort Collins (USA)

Abstract

With the recent rapid development and interest in 3D-printing, the technology is greatly improving, however, challenges such as expanding the material palette available and producing prints with controllable and reproducible properties still remain. For glass 3D-printing, optical properties are key to a print's usefulness and success. Herein we provide a brief overview to direct and indirect methods for glass 3D-printing, describe how printing paste composition influences the opacity of the resulting print and report our efforts to use X-ray micro CT and thermogravimetric analysis to better understand how changes in paste composition lead to the changes in microstructure that are believed to control the bulk glass properties.

Introduction

Interest in additive manufacturing (AM) and 3D-printing (3DP) technology has developed rapidly in recent years, despite having been first conceived more than 30 years ago. Hailed by some as the 'next industrial revolution'[1], [2] such technologies have the potential to change the way products are manufactured and produced and to cause businesses to re-think old supply chains and business models.[3], [4] There are however, still technical challenges for AM and 3DP to face and overcome before these new manufacturing methods can compete with more 'traditional' methods, whatever the business model chosen to distribute the resulting products. These challenges include; reducing long print times, expanding the range of materials available to print with and producing predictable and reproducible material properties.[5] In this paper we will not discuss print times but instead focus on print materials and print properties.

As part of the effort to expand the print materials available for 3DP, we have identified and developed a number of glass printing techniques based upon the kiln glass method first used in ancient Egypt and Mesopotamia.[6], [7] Kiln glass methods place glass pieces (frit) into a mould which is then placed in an oven or furnace and heated so that the glass fuses. This method, rather than the now more commonly used molten glass processing, allows objects to be shaped at room temperature lending itself well to printing. Glass printing methods may be categorised as either direct or indirect.[8] Direct printing includes both powder bed and extrusion printing processes. Here we will focus on a previously developed extrusion printing process [9], [10] building upon the work of Marchelli *et al*.[11] An aqueous paste, comprising of glass frit (particles) and a biopolymer binder, is extruded through a nozzle in the pattern required to build up a 3D object layer by layer. The print is then allowed to dry in air forming greenware which is robust enough to handle but non-functional. The greenware is then fired in a kiln to burn away the binder and fuse the glass particles. Depending upon the temperatures used in the firing cycle, the glass may become a viscous, honey-like liquid and so in some cases will need support in order to retain the desired shape.[8] Indirect printing methods make use of the same glass pastes which, instead of being extruded, are used to fill moulds. These moulds can be made by traditional methods, or using 3DP techniques to either print the mould directly or to print a pattern for the mould. In this way an ABS print could be the pattern for a mould used to cast the same object from a variety of materials. The disadvantage of indirect print methods is however that the design is limited by the need to fill the mould and the extra steps in the build process. Both direct and indirect print methods include elements typically associated with 3DP, such as fused deposition modelling/extrusion printing of a mould, pattern or the print itself, and combine this with traditional glass production techniques to vastly increase the applicability of 3DP in this area without the need for highly specialized equipment.

Glass is often chosen as a building material due to the optical properties it possesses, chief of which is transparency – or controlled transparency. Float glass methods are able to consistently produce high quality, optically transparent glass and there are well established post processing techniques to produce opaque glass with a range of transmission properties.[6], [12] By comparison, it has been found that the kiln glass methods described above show a link between the glass frit (particle) size and the transparency of the resulting object, with smaller particles producing higher resolution but less transparent prints (Figure 1).[13] While there are applications for opaque glass, understanding the cause of and being able to control and predict the opacity of the glass is a priority. Ideally we would want to have the ability to produce a high resolution and highly transparent print.

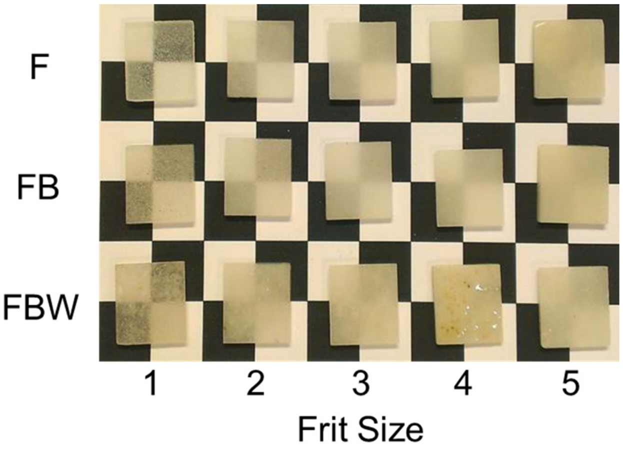

Figure 1 – Uniform fired glass samples produced from frit only (F), frit with powdered HEC binder (FB) and an aqueous paste of frit and HEC binder (FBW). Numbers correspond to the average diameter of the frit used: (1) 150 μm < d < 250 μm, (2) 75 μm < d < 150 μm, (3) 63 μm < d < 75 μm, (4) 38 μm < d < 63 μm, (5) d < 38 μm.[13]

As previously reported, SEM images of the internal structure of the glass (achieved by imaging along fractures in the glass) showed a porous structure which changed with the frit size used.[13] As frit size was decreased it appeared that the pores in the glass became more numerous but smaller. A refractive index change at an interface between glass and air (such as at a pore boundary) will lead to light scattering and so it can be seen that a change in pore structure is likely to have a large effect on the light transmission properties of the glass. It is expected that changes to the glass microstructure will also affect other bulk properties of the glass. This was supported by the measurement of a reduced Young's modulus for the kiln glass samples compared to glass produced using standard techniques. The reduction was consistent with a porosity of < 5 % as observed by SEM.[13], [14] In this paper we will focus on the changes in optical, rather than mechanical, properties associated with varying printing paste compositions and describe our efforts to understand the underlying microstructural differences.

Methodology

Powdered glass frit (soda-lime-silica) 'Crystal Clear, 1401' and kiln-paper was provided by Bullseye Glass. 2-Hydroxyethylcellulose (HEC) was supplied by Sigma Aldrich and used as supplied. Any water used was Millipore filtered unless otherwise stated. The glass powder frit was sieved using an Endecotts Minor Sieve Shaker separating the frit based upon average particle diameter.

Glass pastes were produced by mixing glass frit, binder and water in the ratio 1:0.05:1 by mass. Uniform glass samples (15 mm by 15 mm by 2 mm) were formed by placing either: glass paste, a powdered mix of frit and binder or frit alone, into rectangular moulds and firing according the following firing schedule. (1) temperature ramp of 200ºC/h to 150ºC then hold for 5 minutes, (2) temperature ramp of 430ºC/h to 720ºC then hold for 10 minutes (3) full cool to 510ºC and hold for 30 minutes (4) cool at rate of 80ºC/h to 430ºC and hold for 10 minutes (5) cool to room temperature. The resulting glass was post-processed and cut to uniform dimensions.[13]

Characterisation Techniques

X-ray tomography measurements of the uniform fired glass samples were conducted using a Nikon XT H 225 ST producing images with a voxel size of 4.2 x 4.2 x 4.2 µm. The X-ray tube current and voltage were 130 µA and 140 kV respectively. Each scan contained 1440 projections with 2 frames per projection and took approximately 2 hours to complete. Data analysis was performed using Avizo 8 Fire Edition software.

Thermogravimetric analysis (TGA) was conducted using a TA instruments Q500 thermogravimetric analyser. A platinum sample pan was used and heating cycles were run in air. For samples containing glass frit a kiln-paper holder was also used to prevent the glass sticking to the sample pan. Programmable heating cycles were available allowing both simple heat ramps 10ºC per min to 950ºC, and the full firing cycle described earlier to be performed.

Results

Increasing glass opacity with decreasing particle size and as a function of paste composition has been previously quantified using light transmission measurements, the details of which are given elsewhere.[13] All samples were measured relative to a background of immersion oil (*n*20/D = 1.517), used to eliminate scattering from the glass surface. Here we have converted the resulting percentage light transmission measurements to attenuation coefficients, for a given wavelength, using the Beer-Lambert law (Equation 1), allowing trends to be more easily observed. The resulting attenuation coefficients can be seen in Figure 2.

$$I = I_0 e^{-\alpha z} \quad (1)$$

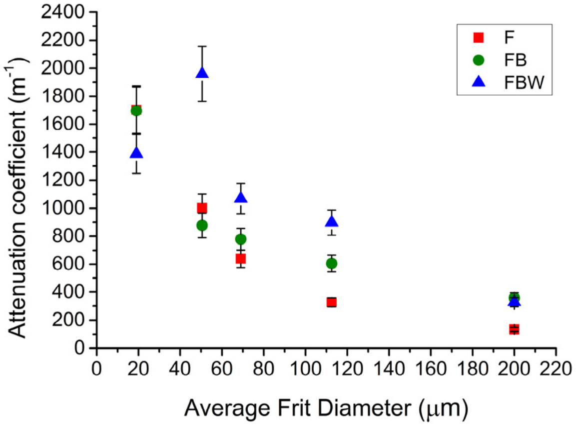

Figure 2 – Attenuation coefficients at 550 nm for samples produced only glass frit (F), frit with HEC binder (FB) and frit with binder and water (FBW).

There is a clear trend showing an increase in attenuation coefficient as the average frit diameter decreases, indicating, as expected, that light transmission decreases with decreasing particle size. Furthermore it can be seen that, with the addition of a binder and then further addition of water, the attenuation coefficient is increased. This shows that not only does the frit size used affect the transparency of the glass but also the addition of binder and water. With this in mind we aimed to further explore the structural changes, previously observed by SEM, linked to paste composition and how these related to the glass transparency.

X-ray micro-tomography was used to obtain information on the glass structure in 3D, observing differences as a function of composition. Figure 3 shows the post-processing of the images which enable the pore structure to be isolated and the properties of the individual pores measured (such as pore area, volume and equivalent diameter – the diameter of a sphere of the same volume). An internal volume of each sample (Figure 3) was chosen for pore analysis to prevent gas external to the sample being mistakenly identified as pores. These results are summarised in Table 1 and the distribution of pore sizes shown in Figure 4.

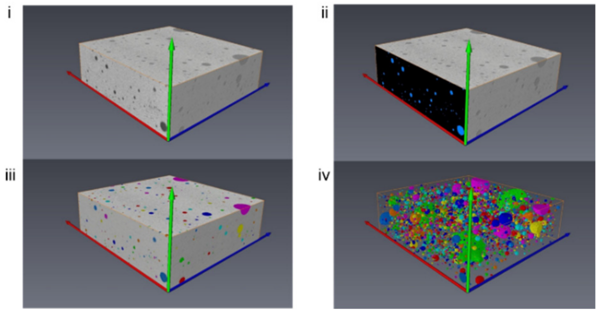

Figure 3 – A 4.3 x 4.1 x 1.4 mm section of a glass sample showing how the pore structure can be reconstructed using tomography scans. The scanned image (i) is first thresholded (ii) to identify areas occupied by glass and those occupied by pores. A morphological opening operator is then applied to remove noise and image artifacts. The areas classed as pores are then able to be identified individually due to the closed pore structure (iii). The regions occupied by glass can then be removed to show the pore structure in 3D (iv). Measurements of the pore area, volume and equivalent diameter can then be performed.

It can be seen in Table 1 that the glass produced using the smaller frit size has a greater number of pores which also occupy a greater volume of the sample and have a greater surface area. This also means that, within the resolution of the technique (12 µm pore diameter), the smaller frit size sample has a lower bulk density. This links well with the transparency of the glass since the sample with the greater number, surface area and volume of pores, therefore with the greatest potential to scatter light, is more opaque.

Table 1 – Summary of pore measurements for glass samples produced from pastes containing frit, HEC binder and water using either frit of average diameter 150 < *d* < 250 µm or *d* < 38 µm.

	250 µm > *d* > 150 µm	38 µm > *d*
Volume of sample measured (µm^3)	2.451x10^{10}	2.451x10^{10}
# of pores	2019	6037
Total pore area (µm^2)	2.38x10^7	7.28x10^7
Total pore vol (µm^3)	6.91x10^8	2.06x10^9
Vol % of pores	2.82	8.38
Density of scanned area* (g/cm^3)	2.32	2.19
Min pore diameter (µm)†	12	12
Max pore diameter (µm) †	701	794
Min pore vol (µm^3)	904	904
Max pore vol (µm^3)	1.80x10^8	2.62x10^8

* Used a glass density of 2.385 g/cm^3 based on pycnometry of glass billet of the same glass type. †This is the equivalent diameter, the diameter of a sphere of the same volume.

The tomograms also allow us to measure the pore size distributions of the two samples. Figure 4 shows the pore size distribution of the two samples normalised by the total number of pores. It can be seen that the distribution of sizes is very similar for the two samples with pore numbers increasing with decreasing diameter. It appears therefore that the main difference between the two is simply the far larger number of pores present in the sample made using a smaller frit size. This story is not complete however, since the resolution of this technique cuts off at a 12 µm pore diameter, meaning that we are left without information on smaller pores in the size range of visible light. These pores will also contribute to the absorption and scattering of light, as described by Mie theory.[15] Furthermore it can be seen that a peak in pore numbers as pore size decreases has not been reached. It could be argued that there would be a minimum favourable pore size below which smaller pores are likely to combine or collapse, resulting in a peak in the size distribution as seen in other similar sintering studies.[16] Identifying where this peak lies and the degree to which this affects the scattering of light in the samples will be the next step in characterising the pore structure of the glass.

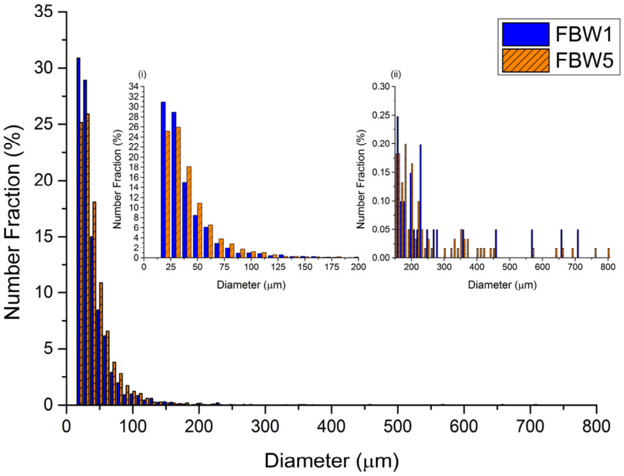

Figure 4 – Pore size distribution, normalised against the total number of pores, for glass samples produced from pastes containing frit, HEC binder and water using either frit of average diameter 150 < d < 250 µm (FBW1) or d < 38 µm (FBW5). Inset (i) shows the smaller particle diameter region in more detail while (ii) shows the larger particle diameter region. Note the varying y axis scales. Diameter values shown are the calculated equivalent diameter.

Returning to the attenuation coefficient measurements for the different samples in Figure 2, we found that there were two factors affecting the transparency of the glass; frit size and the presence of HEC binder. To investigate the significance of the binder to this effect, thermogravimetric analysis (TGA) of the pastes was performed to determine whether any binder remains within the glass after firing.

It had been assumed that during the firing process the organic binders would undergo thermal decomposition reactions forming CO$_2$, CO and other volatile bi-products,[17] which would escape from the glass as part of a de-binding process. To confirm this, a series of thermogravimetric studies were performed. Firstly HEC binder was exposed to a heat ramp from R.T. up to 950 °C at 10 °C/min as a control. The results of this measurement can be seen in Figure 5. Initially there is a small reduction in mass (~ 5 %) associated with dehydration of the sample. There are then two clear stages of mass loss, 220 – 400 °C and 660 – 700 °C. By the end of the heating cycle 1.4% of the starting mass still remains (the char yield), in contrast to the initial assumption that all the organic component would be removed. Similar behavior has also been observed in other TGA studies of HEC undergoing thermal decomposition in air, however the exact temperature ranges during which decomposition takes place and the char yield observed varies between studies. This is likely due to variation in the molecular weight of the polymer tested and the heating rate applied. These studies suggest that the presence of the hydroxyethyl group increases the thermal stability of the polymer, hence increasing the char yield compared to other similar cellulose ethers. [18], [19]

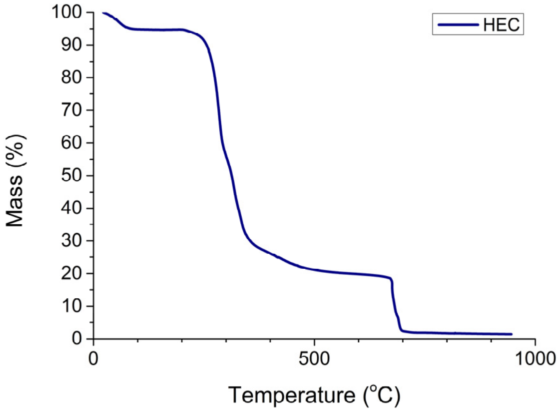

Figure 5 – TGA results showing the percentage mass lost for HEC powder when heating from 0 – 950°C at 10°C/min

Having seen incomplete combustion with HEC alone, we then wanted to observe how this behaviour differed in a full paste system. Before a full paste could be run, a series of controls were needed to allow different components of the system to be identified and discounted from the full paste TGA run. These controls consisted of kiln paper (used to protect the sample pan from the glass), kiln paper with glass frit and the previously discussed HEC run. Kiln paper has an organic component and was found to partially decompose, when kiln paper and frit were run together the results showed mass loss associated with the kiln paper with no mass lost by the frit, as expected. Figure 6 shows the results of TGA measurements for a glass paste ($d < 38$ µm) undergoing a typical firing cycle. There is an initial rapid loss of mass associated with the loss of water, followed by two stepwise decreases in mass in the region expected for both HEC and the kiln paper, based upon previous control measurements.

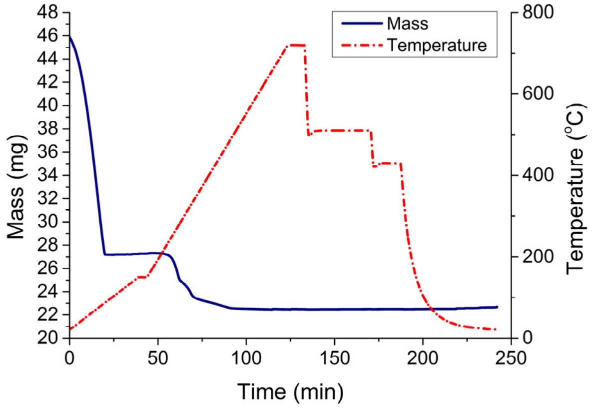

Figure 6 – TGA temperature cycle and mass measurements for a paste using average frit diameter d < 38 µm.

Based upon the control measurements, we made certain assumptions in the analysis of the glass paste measurements. Firstly, that all the water in the paste will be lost in the duration of the firing cycle (approx. 4 hours), secondly that the frit will not lose any mass and thirdly that the kiln paper used to contain the sample will lose the same percentage mass as in the control run. This means that any additional mass lost must be due to loss of HEC. As a result, we find that, for a glass paste containing frit of average diameter $d < 38$ µm, only 18 % of the original HEC is lost during the firing cycle. This leads to HEC or HEC bi-products representing a low but not insignificant percentage of the total remaining mass (3.9%). This mass loss is greatly reduced compared to that observed for the HEC control.

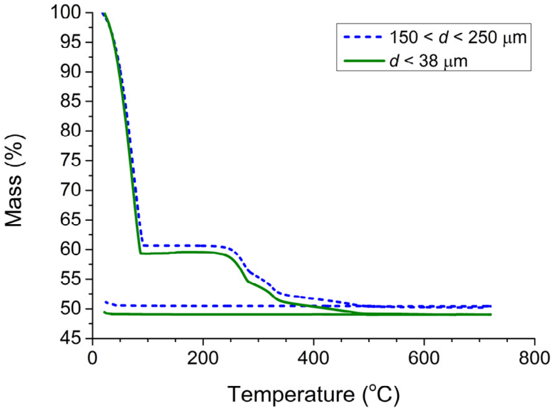

Figure 7 – Comparison of pastes using frit with average diameters of d < 38 µm (green) or 150 <d < 250 µm (blue). Data not corrected for the mass lost by the kiln paper lining the sample holder.

When we now compare pastes produced using different glass frit sizes, as in Figure 7, we find that the overall trends are the same with mass loss occurring in the same temperature regimes. However, the overall percentage mass loss for the paste produced using larger frit size ($150 < d < 250$ µm) is slightly less. We attribute this to slight variance in the initial water content and differing kiln paper to paste mass ratios. Conducting the same analysis as above on the larger frit size, making the same assumptions, we find that the percentage of HEC lost in this system is much greater at 41%.

As a result of these investigations we find that in all pastes with binder present, the resulting glass will also contain binder residue to a varying degree. The fact that residue remains, links well with the increased attenuation coefficients observed for glass produced using binder. In addition the observation that the amount of binder that remains in the glass is larger with smaller frit sizes, once again shows the importance of frit size to the transparency. Not only does frit size directly impact the pore structure and reduce transparency (seen in samples without binder present) but it also affects the amount of binder residue retained in the glass structure if binder is used.

At this stage it is too early to provide a definitive answer as to the why using a smaller frit size should reduce the percentage of binder mass removed, however, it could be that the effects leading to increased total pore volume seen in the tomograms could also be linked to the reduced de-binding (burn off). Other than gas initially trapped within the pastes during mixing and processing, the other main contributor to gas within the pastes will be as a result of the volatile products of binder decomposition. If less of the volatile products are able to escape from the glass during firing then we would expect there to be a greater pore volume and also a greater mass (attributed to the binder) still present within the glass, as has been observed. It might be that the use of smaller frit sizes within the pastes pack more closely, have a larger surface area and so provide a more complex path to the surface of the print for any trapped volatile products. A more complex path would result in a longer travel time to the surface and so, in the limited time available during the firing cycle, a reduction in the quantity of gas that can be expelled. This is however highly speculative and further work, such as producing tomograms of samples before, during and after firing to observe pore development and gas movement within the glass, must be done to investigate this phenomenon.

Conclusion and summary

It is possible to use glass as a material for 3D-printing using either direct or in-direct printing methods however producing prints with controlled and reproducible properties such as opacity is still a challenge. X-ray micro CT shows that there is a link between the glass particle size used in the printing paste and the total pore volume in the print but, at the resolution available, does not appear to alter the distribution of pore sizes. TGA measurements show that the binder used in the printing does not completely burn off as previously expected instead remaining in the print as a further source of light scattering.

Acknowledgements

Our thanks to: Dr A. Rhead and C. Ball at the University of Bath for performing X-ray CT scans and for access to analysis software, Dr G. Whittle and D Hayward (Manners Group, School of Chemistry, University of Bristol) for advice, training and use of TGA equipment.

References

[1] J. D. Prince, “3D Printing: An Industrial Revolution,” *J. Electron. Resour. Med. Libr.*, vol. 11, no. 1, pp. 39–45, Jan. 2014.

[2] B. Berman, “3-D printing: The new industrial revolution,” *Bus. Horiz.*, vol. 55, no. 2, pp. 155–162, Mar. 2012.

[3] G. Brooks, K. Kinsley, and T. Owens, “3D Printing As A Consumer Technology Business Model,” *Int. J. Manag. Inf. Syst.*, vol. 18, no. 4, pp. 271–280, 2014.

[4] F. T. Piller, C. Weller, and R. Kleer, “Business Models with Additive Manufacturing - Opportunities and Challenges from the Perspective of Economics and Management,” in *Advances in Production Technology*, C. Brecher, Ed. 2015, pp. 39–48.

[5] S. Klein, G. Adams, F. Dickin, and S. Simske, “3D Printing: When and Where Does It Make Sense?,” *HP Tech Rep.*, vol. HPL-2013, no. 51, 2013.

[6] E. Le Bourhis, *Glass*, First. WILEY-VCH Verlag, 2008.

[7] W. Vogel, *Chemistry of Glass*. Westerville, Ohio: The American Ceramic Society, 1985.

[8] S. Klein, M. P. Avery, R. Richardson, P. Bartlett, R. Frei, and S. Simske, “3D printed glass: surface finish and bulk properties as a function of the printing process,” in *Proc. SPIE*, 2015, vol. 9398, p. 93980R–93980R–9.

[9] S. Klein, S. Simske, C. Parraman, P. Walters, D. Huson, and S. Hoskins, “3D Printing of Transparent Glass,” *HP Tech Rep.*, vol. HPL-2012, no. 198, 2012.

[10] S. Klein, F. Dickin, G. Adams, and S. Simske, “Glass : an old material for the future of manufacturing,” *HP Tech Rep.*, vol. HPL-2012, no. 230, 2012.

[11] G. Marchelli, R. Prabhakar, D. Storti, and M. Ganter, “The guide to glass 3D printing: developments, methods, diagnostics and results,” *Rapid Prototyp. J.*, vol. 17, no. 3, pp. 187–194, 2011.

[12] N. . Min’ko, V. S. Bessmertnyi, V. A. Panasenko, S. V. Semenenko, S. N. Zubenko, and N. I. Voloshko, “Frosting as a contemporary method of glass decoration,” *Glas. Ceram.*, vol. 60, pp. 161–163, 2003.

[13] M. P. Avery, S. Klein, R. Richardson, P. Bartlett, G. Adams, F. Dickin, and S. Simske, “The Rheology of Dense Colloidal Pastes Used in 3D-Printing,” in *NIP & Digital Fabrication Conference*, vol. 2014.

[14] J. A. Choren, S. M. Heinrich, and M. B. Silver-Thorn, “Young’s modulus and volume porosity relationships for additive manufacturing applications,” *J. Mater. Sci.*, vol. 48, no. 15, pp. 5103–5112, Apr. 2013.

[15] H. C. van de Hulst, *Light Scattering by Small Particles*. Courier Corporation, 1957.

[16] M. D. SACKS and T.-Y. TSENG, “Preparation of SiO 2 Glass from Model Powder Compacts: II, Sintering,” *J. Am. Ceram. Soc.*, vol. 67, no. 8, pp. 532–537, Aug. 1984.

[17] P. Tomasik, M. Pałasiński, and S. Wiejak, *Advances in Carbohydrate Chemistry and Biochemistry Volume 47*, vol. 47. Elsevier, 1989.

[18] X. G. Li, M. R. Huang, and H. Bai, “Thermal decomposition of cellulose ethers,” *J. Appl. Polym. Sci.*, vol. 73, pp. 2927–2936, 1999.

[19] L. M. Zhang and L. Q. Chen, “Water-soluble grafted polysaccharides containing sulfobetaine groups: Synthesis and characterization of graft copolymers of hydroxyethyl cellulose with 3-dimethyl(methacryloyloxyethyl)ammonium propane sulfonate,” *J. Appl. Polym. Sci.*, vol. 83, pp. 2755–2761, 2002.

Author Biography

Michael Avery received his MSci in Chemical Physics with Industrial Experience from the University of Bristol (2012). He is currently a PhD student at the Bristol Centre for Functional Nanomaterials where he is researching new silica-based materials for 3D-printing.